Available online at www.sciencedirect.com
SCIENCE DIRECT
International Journal of Heat and Mass Transfer 49 (2006) 1907–1914
International Journal of HEAT and MASS TRANSFER
www.elsevier.com/locate/ijhmt

An analytical study of local thermal equilibrium in porous heat sinks using fin theory

Tzer-Ming Jeng [a], Sheng-Chung Tzeng [b,*], Ying-Huei Hung [c]

[a] Department of Mechanical Engineering, Air Force Institute of Technology, GangShan 820, Taiwan, ROC
[b] Department of Mechanical Engineering, Chienkuo Technology University, No. 1, Chieh Shou N Road, Chang Hua 500, Taiwan, ROC
[c] Department of Power Mechanical Engineering, National Tsing Hua University, Hsinchu 300, Taiwan, ROC

Received 21 February 2005; received in revised form 8 November 2005
Available online 10 January 2006

Abstract

This work presents an algorithm model for estimating the heat transfer by forced convection of the porous heat sink in a channel by applying the fin theory and the concept of the thermal network. The proposed algorithm model is simpler and more convenient than numerical analysis. By comparison with numerical calculations and other experiments, the model was verified to predict accurately heat transfer in various porous channels, such as metal foam channels and sintered porous channels. The inlet thermal boundary condition is also examined. The finding reveals that the effect of the inlet thermal boundary condition on the numerical calculations becomes weaker as the interstitial heat transfer coefficient increases. Additionally, a parameter Ω in terms of h_v, k_s^* and H^* is postulated to determine the local thermal equilibrium (LTE) in porous channels. Analytical results reveal some criteria for LTE in various porous channels. For instance, the criterion for LTE in aluminum foam channels is: if $\varepsilon = 0.91$ and $H = 45$ mm, $Re \geqslant 4700$; if $\varepsilon = 0.95$/10PPI and $H = 45$ mm, $Re \geqslant 1600$; if $\varepsilon = 0.95$/10PPI and $H = 25.4$ mm, then $Re \geqslant 6600$. Besides, the scope of LTE in sintered copper bead porous channels with $\varepsilon = 0.38/d = 1.59$ mm and $H = 10$ mm is about $Re \geqslant 6600$. Accordingly, the one-equation model, which is simpler than the two-equation model, can be used to analyze heat transfer through porous media in the applicable regions.

Keywords: Heat transfer; Porous heat sinks; Fin theory; Local thermal equilibrium

1. Introduction

The electronics industry is manufacturing denser and more powerful products, necessitating a better cooling technology. Many cooling devices involve channels filled with porous heat sinks. The use of porous heat sinks in the electronics cooling provides two advantages. First, the porous heat sink provides more than 10 times the contact area of a smooth surface. A higher surface area facilitates convection to the fluid stream. Second, the irregular structure of the porous heat sinks, at sufficiently high velocities, causes irregular fluid flow, increasing the thermal dispersion conductivity.

Many investigators have investigated the thermal characteristics of porous heat sinks in rectangular channels. Hunt and Tien [1] experimentally measured forced convection in foam material channels. They also numerically simulated the thermal characteristics by applying the one-equation model. Chou et al. [2] numerically and experimentally studied forced convection in horizontal square channels through packed spheres. The one-equation model was also used in numerical simulations. Besides, Hwang and Chao [3] and Hwang et al. [4] reported heat transfer measurements for sintered copper bead porous channels, and numerically solved the two-equation model that yielded accurate predictions. They also examined the effect of the inlet thermal boundary condition on the numerical

* Corresponding author. Tel.: +886 4 711 1111x3132; fax: +886 4 735 7193.
E-mail addresses: tsc@ctu.edu.tw, tsc33@ms32.hinet.net (S.-C. Tzeng).

0017-9310/$ - see front matter © 2005 Published by Elsevier Ltd.
doi:10.1016/j.ijheatmasstransfer.2005.11.012

Nomenclature

C_1	parameter for inlet thermal boundary condition
C_F	inertial coefficient of the porous heat sink
C_p	specific heat of fluid at constant pressure (J/kg/°C)
d	diameter of fiber or sphere of the porous heat sink (m)
d_p	pore diameter of the porous heat sink (m)
Da	Darcy number, $K/(2H)^2$
H	height of the porous heat sink (m)
h	heat transfer coefficient (W/m^2/°C)
h_v	interstitial heat transfer coefficient (W/m^3/°C)
h_{fw}	heat transfer coefficient between the fluid stream and the heated wall (W/m^2/°C)
K	permeability of the porous heat sink (m^2)
k	thermal conductivity (W/m °C)
L	length of the porous heat sink (m)
Nu_b	Nusselt number based on bulk mean fluid temperature, Eqs. (12) and (30)
Nu_i	Nusselt number based on inlet fluid temperature, Eqs. (13) and (29)
Pr	Prandl number, Eq. (8)
q_w	heat flux of heated wall (W/m^2)
Re	Reynolds number, $\rho_f u_i 2H/\mu$
T	temperature (°C)
u	fluid flow velocity in the streamwise direction (m/s)
U	dimensionless fluid flow velocity in the streamwise direction
v	fluid flow velocity in the crosswise direction (m/s)
V	dimensionless fluid flow velocity in the crosswise direction
W	width of the porous heat sink (m)
x, y	Cartesian coordinates (m)
X, Y	dimensionless Cartesian coordinates

Greek symbols

ε	porosity of the porous heat sink
η	effective fin efficiency
μ	viscosity of fluid (kg/m/s)
θ	dimensionless temperature, $(T - T_i)/(q_w H/k_f)$
ρ	density (kg/m^3)
ω	vorticity
Ω	parameter for local thermal equilibrium
Ψ	stream function

Superscript

*	effective

Subscripts

d	thermal dispersion
f	fluid
i	at the channel inlet
s	solid matrix
w	channel wall

predictions. Ichimiya [5] studied the thermal behavior in the ceramic-foam channel and presented a new method that applies the two-equation model to estimate the heat transfer between fluid and solid material. Calmidi and Mahajan [6] experimentally investigated the forced convection in highly porous aluminum foams, using air as the cooling fluid. They also developed a numerical model by assuming non-thermal equilibrium between the fluid stream and the solid matrix. All of these works applies the porous approach to perform numerical analyses. Much computer time is required because many numerical iterations are required. The porous medium is composed of numerous regularly arranged fibers or spheres, in what can be considered to be a fin structure. Hence, an algorithm model for predicting thermal performance using fin theory may be developed.

This work seeks to elucidate an algorithm model to estimate the heat transfer of the porous heat sink in a channel by applying the fin theory. Comparisons were made with the numerical calculations using the porous method and other experimental data, to verify the accuracy and reliability of the presented algorithm model. Additionally, the parameters required to specify the inlet thermal boundary condition and the local thermal equilibrium (LTE) are elucidated with reference to the presented algorithm model. A parameter (Ω) in terms of h_v, k_s^* and H^* specifies the LTE of the porous channels. When the LTE has been specified, the regions to which the one-equation model can be applied in practical problems that involve the aluminum foam media and sintered copper bead porous media are presented. Therefore, the one-equation model, which is simpler than the two-equation model, can be used to analyze heat transfer through porous media in the regions of applicability.

2. Thermal network model

Fig. 1 presents the physical configuration used in this model. A porous medium with uniform porosity is fully confined in a rectangular channel, which is symmetrically or asymmetrically heated through its top and bottom surfaces. The overall heat transfer mechanism in this porous channel can be analyzed using the thermal network concept, as shown in Fig. 2. Two parallel heat transfer paths through the channel wall transfer heat into the fluid stream. One is an indirect path through the solid matrix; the other is a direct path to the fluid stream. The mechanism of heat transfer through the indirect path through the solid matrix is an initial transfer of heat from the channel wall to the

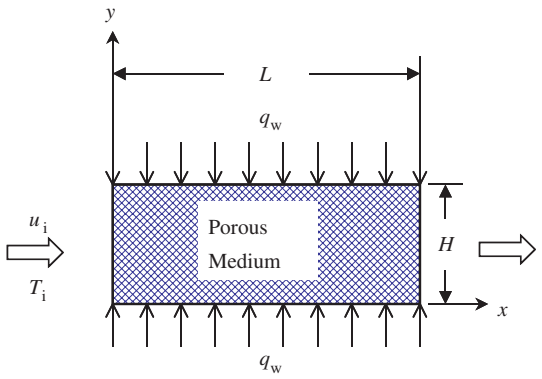

Fig. 1. Physical configuration.

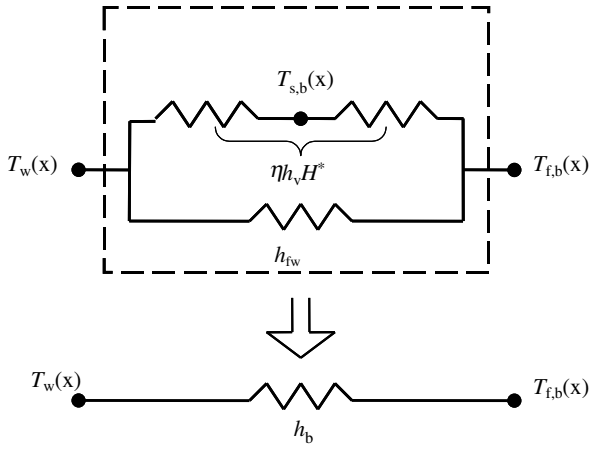

Fig. 2. Schematic of thermal network model.

solid matrix by conduction, and then a transfer of heat in the solid matrix to the fluid stream by convection. The mechanism of the transfer of heat through the direct path is the direct transfer of heat from the channel wall to the fluid stream by convection. Accordingly, the fin theory presented by Holman [7] was used to determine the heat flux dissipated from the heated wall surfaces, as follows:

$$q_w(x) = h_v H^*[T_{s,b}(x) - T_{f,b}(x)] + h_{fw}[T_w(x) - T_{f,b}(x)] = (\eta h_v H^* + h_{fw})[T_w(x) - T_{f,b}(x)] \quad (1)$$

where

$$\eta = 0 \quad \text{for LTE}$$
$$= \frac{\tanh(mH^*)}{mH^*} \quad \text{for non-LTE} \quad (2)$$

$$m = \sqrt{\frac{h_v}{k_s^*}} \quad (3)$$

$$H^* = H/2 \quad \text{when both wall surfaces were heated}$$
$$= H \quad \text{when one wall surface was heated} \quad (4)$$

$$h_{fw} = Nu_{b,\varepsilon=1} \cdot (k_f^* + k_d + k_s^*)/2H \quad \text{for LTE}$$
$$= Nu_{b,\varepsilon=1} \cdot k_f^*/2H \quad \text{for non-LTE} \quad (5)$$

where h_v is the interstitial heat transfer coefficient between the solid matrix and the fluid; h_{fw} represents the fluid–wall heat transfer coefficient along the path of directly heat transfer; η is the effective fin efficiency; k_s^* is the effective solid matrix conductivity; H is the height of the porous material, and the $Nu_{b,\varepsilon=1}$ is the Nusselt number based on the bulk mean temperature in an empty channel. The fluid flow in porous channels is more like slug flow than parabolic flow, and was investigated by Hunt and Tien [1]. Therefore, the correlation specified by $Nu_{b,\varepsilon=1}$ for the slug flow at the thermal entrance region of the parallel-plate channel with uniform heat flux is considered. The correlation at $Nu_{b,\varepsilon=1}$, Eq. (6), is obtained from numerical solutions for various streamwise locations, channel heights, Reynolds numbers and Prandtl numbers. The following section introduces the appropriate numerical model. This correlation is shown below:

$$Nu_{b,\varepsilon=1} = \xi\left[1.383(X^*)^{-0.45}\right] \quad \text{for } X^* \leqslant 0.001$$
$$= \xi\left[12 + 22(10^3 X^*)^{-0.506}\exp(-164X^*)\right] \quad \text{for } X^* > 0.001 \quad (6)$$

where

$$\xi = 1 \quad \text{for both wall surfaces with isoflux heating}$$
$$= 0.5 \quad \text{for one wall surface with isoflux heating} \quad (7)$$

$$Re = \frac{\rho_f u_i 2H}{\mu}, \quad Pr = \frac{\mu/\rho_f}{k_f/(\rho C_p)_f}, \quad Da = \frac{K}{(2H)^2},$$

$$Pr^* = \frac{\mu/\rho_f}{k_f^*/(\rho C_p)_f}, \quad Pr^{**} = \frac{\mu/\rho_f}{(k_f^* + \overline{k_d} + k_s^*)/(\rho C_p)_f} \quad (8)$$

$$X^* = \frac{x/2H}{RePr^{**}} \quad \text{for LTE}$$
$$= \frac{x/2H}{RePr^*} \quad \text{for non-LTE} \quad (9)$$

$$k_f^* = \varepsilon k_f, \quad k_s^* = \text{measured data} \quad (10)$$

$$\overline{k_d} = 0.06RePr\sqrt{Da}k_f \quad \text{for porous foam channels}$$
$$= 1 + 3d/H[\exp(-H/3d) - 1] \quad \text{for packed-sphere channels} \quad (11)$$

The thermal dissipation conductivity in Eq. (11) is the mean value. The relevant correlations are presented in Refs. [4,6]. Now,

$$Nu_b = (\eta h_v H^* + h_{fw}) \cdot 2H/k_f \quad (12)$$

$$Nu_i = \left(\frac{1}{Nu_b} + \frac{x}{RePrH^*}\right)^{-1} \quad (13)$$

3. Numerical analysis

3.1. Basic assumptions and governing equations

The side walls of the channel are both insulated; accordingly, this is essentially a two-dimensional problem. The

heating surface is isoflux. The other assumptions and simplifications are as follows: (1) the porous medium is homogenous and isotropic; (2) the fluid flow is in the steady state, laminar and incompressible; (3) the thermophysical properties of the fluid and porous media are constant; (4) a local non-thermal equilibrium exists between the porous media and the fluid stream. Hence, the governing equations are presented as follows:

$$\frac{\partial u}{\partial x}+\frac{\partial v}{\partial y}=0 \tag{14}$$

$$\frac{\rho_f}{\varepsilon^2}\left(u\frac{\partial u}{\partial x}+v\frac{\partial u}{\partial y}\right)=-\frac{\partial p}{\partial x}-\frac{\mu_f}{K}u-\frac{\rho_f C_F}{\sqrt{K}}|\vec{V}|u+\frac{\mu_f}{\varepsilon}\left(\frac{\partial^2 u}{\partial x^2}+\frac{\partial^2 u}{\partial y^2}\right) \tag{15}$$

$$\frac{\rho_f}{\varepsilon^2}\left(u\frac{\partial v}{\partial x}+v\frac{\partial v}{\partial y}\right)=-\frac{\partial p}{\partial y}-\frac{\mu_f}{K}v-\frac{\rho_f C_F}{\sqrt{K}}|\vec{V}|v+\frac{\mu_f}{\varepsilon}\left(\frac{\partial^2 v}{\partial x^2}+\frac{\partial^2 v}{\partial y^2}\right) \tag{16}$$

$$(\rho C_p)_f\left(u\frac{\partial T_f}{\partial x}+v\frac{\partial T_f}{\partial y}\right)=h_v(T_s-T_f)+\frac{\partial}{\partial x}\left[(k_f^*+k_d)\frac{\partial T_f}{\partial x}\right]+\frac{\partial}{\partial y}\left[(k_f^*+k_d)\frac{\partial T_f}{\partial y}\right] \tag{17}$$

$$0=h_v(T_f-T_s)+\frac{\partial}{\partial x}\left(k_s^*\frac{\partial T_s}{\partial x}\right)+\frac{\partial}{\partial y}\left(k_s^*\frac{\partial T_s}{\partial y}\right) \tag{18}$$

The above equations can be non-dimensionalized by introducing the following variables:

$$X=\frac{x}{H},\quad Y=\frac{y}{H},\quad U=\frac{u}{u_i},\quad V=\frac{v}{u_i},$$
$$Pr=\frac{\mu/\rho_f}{k_f/(\rho C_p)_f},\quad Da=\frac{K}{(2H)^2},\quad Re=\frac{\rho_f u_i 2H}{\mu},$$
$$U_M=\frac{\sqrt{u^2+v^2}}{u_i},\quad \theta=\frac{T-T_i}{q_w H/k_f},\quad Nu_{fs}^*=\frac{h_v H^2}{k_f} \tag{19}$$

Additionally, the variables were changed to replace the velocity components with the vorticity, ω, and the stream function, ψ.

$$\omega=-\frac{\partial U}{\partial Y}+\frac{\partial V}{\partial X},\quad \partial U=\frac{\partial \Psi}{\partial Y},\quad \partial V=-\frac{\partial \Psi}{\partial X} \tag{20}$$

The vorticity-transport equation is obtained. The dimensionless governing equations are then,

$$-\omega=\frac{\partial^2\Psi}{\partial X^2}+\frac{\partial^2\Psi}{\partial Y^2} \tag{21}$$

$$U\frac{\partial\omega}{\partial X}+V\frac{\partial\omega}{\partial Y}=-\frac{\varepsilon^2}{2Re\cdot Da}\omega-\frac{\varepsilon^2 C_F U_M}{2\sqrt{Da}}\omega+\frac{\varepsilon^2 C_F}{2\sqrt{Da}}\left(U\frac{\partial U_M}{\partial Y}-V\frac{\partial U_M}{\partial X}\right)+\frac{2\varepsilon}{Re}\left(\frac{\partial^2\omega}{\partial X^2}+\frac{\partial^2\omega}{\partial Y^2}\right) \tag{22}$$

$$U\frac{\partial\theta_f}{\partial X}+V\frac{\partial\theta_f}{\partial Y}=\frac{2Nu_{fs}^*}{Re\cdot Pr}(\theta_s-\theta_f)+\frac{2}{Re\cdot Pr}\left\{\frac{\partial}{\partial X}\left[\left(\frac{k_f^*+k_d}{k_f}\right)\frac{\partial\theta_f}{\partial X}\right]+\frac{\partial}{\partial Y}\left[\left(\frac{k_f^*+k_d}{k_f}\right)\frac{\partial\theta_f}{\partial Y}\right]\right\} \tag{23}$$

$$0=Nu_{fs}^*(\theta_f-\theta_s)+\frac{k_s^*}{k_f}\left(\frac{\partial^2\theta_s}{\partial X^2}+\frac{\partial^2\theta_s}{\partial Y^2}\right) \tag{24}$$

3.2. Boundary conditions

Roache [8] presented the boundary conditions for the vorticity-transport equation; the relevant boundary conditions are assumed to be as follows:

$$\text{at } X=0:\quad \Psi=Y,\quad \omega=\frac{-\partial^2\Psi}{\partial X^2},\quad \theta_f=0,\quad -\frac{k_s^*}{k_f}\frac{\partial\theta_s}{\partial X}=Nu_{fs}^*C_1(\theta_f-\theta_s) \tag{25}$$

$$\text{at } X=L/H:\quad \frac{\partial^2\Psi}{\partial X^2}=0,\quad \frac{\partial\omega}{\partial X}=0,\quad \frac{\partial\theta_f}{\partial X}=\frac{4}{Re\cdot Pr},\quad Nu_{fs}^*(\theta_s-\theta_f)=\frac{k_s^*}{k_f}\left(\frac{\partial^2\theta_s}{\partial Y^2}\right) \tag{26}$$

$$\text{at } Y=0:\quad \Psi=0,\quad \omega=-\frac{\partial^2\Psi}{\partial Y^2},\quad \theta_f=\theta_s,\quad -1=\frac{k_f^*}{k_f}\frac{\partial\theta_f}{\partial Y}+\frac{k_s^*}{k_f}\frac{\partial\theta_s}{\partial Y} \tag{27}$$

$$\text{at } Y=1:\quad \Psi=1,\quad \omega=-\frac{\partial^2\Psi}{\partial Y^2},\quad \theta_f=\theta_s,\quad 1=\frac{k_f^*}{k_f}\frac{\partial\theta_f}{\partial Y}+\frac{k_s^*}{k_f}\frac{\partial\theta_s}{\partial Y} \tag{28}$$

Notably, C_1 in the boundary condition of the solid matrix temperature at the channel inlet is determined empirically. The value of C_1 generally depends on the structure of the porous medium.

3.3. Thermophysical properties

Table 1 lists some porous properties and empirical correlations for air-flow across porous channels. The effective conductivity of the solid k_s^* is a function of the geometry and the solid conductivity k_s. The effective conductivity of the fluid k_f^* can be expressed in simple form as εk_f.

3.4. Numerical procedure

The governing equation was discretized using the power-law scheme. The stream function equation and vorticity-transport equation are solved simultaneously by iterations. The velocity components U and V are determined from the stream function. When the velocity components have been determined, the energy equation can be solved to obtain the temperature distribution. All discretized algebraic equations are solved using the SIS algorithm developed by Lee [12]. The solutions are confirmed by varying the

Table 1
List of h_v empirical correlations for air-flow across porous channels

Authors	Porous material	k_s^* (W/m °C)	ε	PPI	d (mm)	d_p (mm)	$L/W/H$ (mm)	D_h (mm)	K (m^2), F	h_v correlation
Hwang et al. [9]	Al foam	4.10[a]	0.95	10	0.36	2.03	60/60/25.4	35.69	$K = 7.5E{-}8$, $F = 0.065$,	$Nu_{dp} = (h_v d_p^2)/k_f = 0.3248 Re_{dp}^{0.601}$, for $Re_L = u_i L/\nu = 1900$–7800
Calmidi and Mahajan [6]	Al foam	2.48[a]	0.973	5	0.5	4.02	114/63/45	52.5	$K = 2.7E{-}7$, $F = 0.097$	$Nu_{fs} = h_{fs} d/k_f = 0.52(u_i d/\varepsilon\nu)^{0.5} Pr^{0.37}$,
		4.10[a]	0.949	10	0.4	3.13			$K = 1.2E{-}7$, $F = 0.097$	$a_{fs} = 3\pi(\beta d)/(0.59 d_p)^2$, $\beta = 1 - \exp[-(1-\varepsilon)/0.04]$,
		3.71[a]	0.955	20	0.3	2.70			$K = 1.3E{-}7$, $F = 0.093$	$h_v = h_{fs} a_{fs}$, for $Re_L = u_i L/\nu = 5940$–$29{,}710$
		6.46[a]	0.912	5	0.55	3.80			$K = 1.8E{-}7$, $F = 0.085$	
		6.37[a]	0.913	40	0.25	1.80			$K = 0.53E{-}7$, $F = 0.084$	
Ichimiya [5]	Ceramic foam	3.38[b]	0.875	20	None	1.3	300/300/30	54.55	$K = 2.2E{-}7$, $F = 0.162$	$Nu_{dp} = (h_v d_p^2)/k_f = 2.43 Re_{dp}^{0.42}$, for $Re_{dp} = u_d d_p/\nu = 65$–$457$ [10]
Hwang et al. [4]	Sintered bronze beads	10.57[b]	0.37	None	0.72	0.61	50/50/10	16.67	$K = 2.9E{-}10$, $F = 0.242$,	$Nu_d = (h_v d^2)/k_f = 0.0814(1-\varepsilon)\varepsilon^2$ $(d_p/d)^{0.35} Pr^{0.33} Re_d^{1.35}$ for $Re_d = u_d d_p/\nu \leqslant 75$
		10.29[b]	0.38		1.59	1.29			$K = 1E{-}9$, $F = 0.118$	$Nu_d = 21.65(1-\varepsilon)\varepsilon^2 Pr^{0.33} Re_d^{0.59}$ for $Re_d \geqslant 350$

Note: The superscript 'a' means the k_s^* is obtained by using $k_s^* = 0.181(1-\varepsilon)^{0.763} k_s$ [11]; 'b' means the k_s^* is measured data.

grid spacing and the convergence criterion. The number of grid-cells in the flow direction is 121, and that perpendicular to the flow is 31. The convergence criterion is $\mathrm{Max}\left|\left(F^{(n)} - F^{(n-1)}\right)/\left(F_{\max}^{(n)} - F_{\min}^{(n)}\right)\right| \leqslant 1 \times 10^{-6}$, where F is Ψ, ω, θ_f or θ_s. The numerical results are verified by varying the length of the computational domain to ensure the validity of the boundary condition at the exit. The ratio L/H should be sufficiently large to allow the local bulk Nusselt numbers (Nu_b) in the streamwise direction to approach a constant value. This follows from the assumption that the thermal fully developed boundary condition at the exit is suitable. The numerical results for the inlet Nusselt number (Nu_i) and the bulk Nusselt number (Nu_b) on the channel wall are defined by

$$Nu_i = \frac{q_w 2H}{k_f(T_w - T_i)} = -2\left(\frac{k_s^*}{k_f}\frac{\partial\theta_s}{\partial Y} + \frac{k_f^*}{k_f}\frac{\partial\theta_f}{\partial Y}\right)\Big/\theta_w \tag{29}$$

$$Nu_b = \frac{q_w 2H}{k_f(T_w - T_{fb})} = -2\left(\frac{k_s^*}{k_f}\frac{\partial\theta_s}{\partial Y} + \frac{k_f^*}{k_f}\frac{\partial\theta_f}{\partial Y}\right)\Big/\left(\frac{\int_0^1 \theta_f u\,dY}{u_i}\right) \tag{30}$$

4. Results and discussion

4.1. Validity of numerical calculation

Fig. 3 compares the numerical prediction with the previous correlation for parallel-plate channels, to validate the numerical calculation. Fig. 3 plots the bulk Nusselt number as a function of $X/(Re \cdot Pr)$. The numerical prediction is very consistent with the correlation obtained by Shah and London in Ref. [13] for parabolic flow,

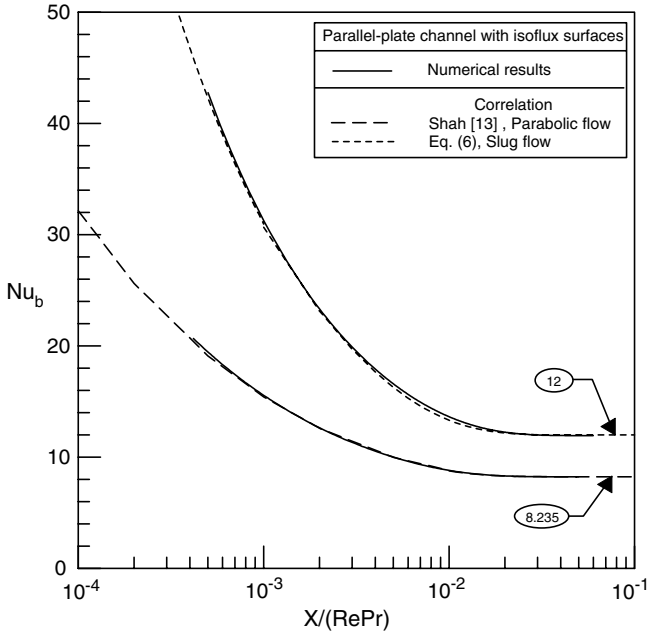

Fig. 3. Bulk Nusselt number as a function of $X/(Re\,Pr)$ for parallel-plate channels.

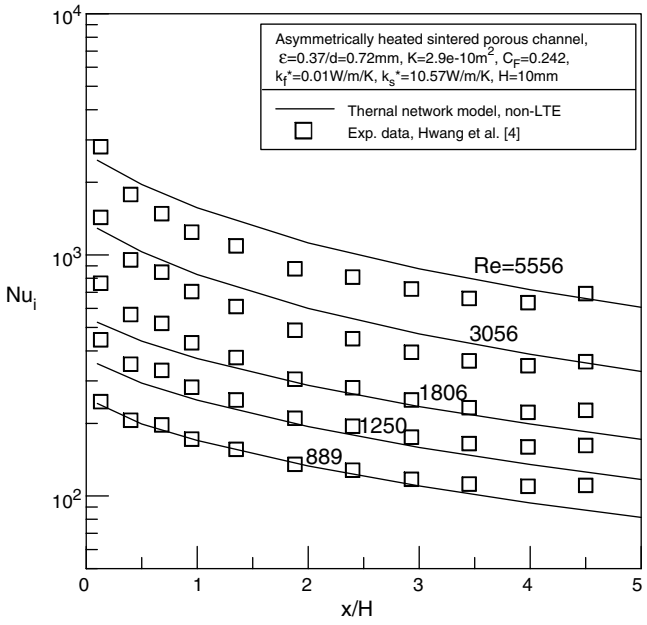

Fig. 4. Prediction of local Nusselt number in the sintered porous channel.

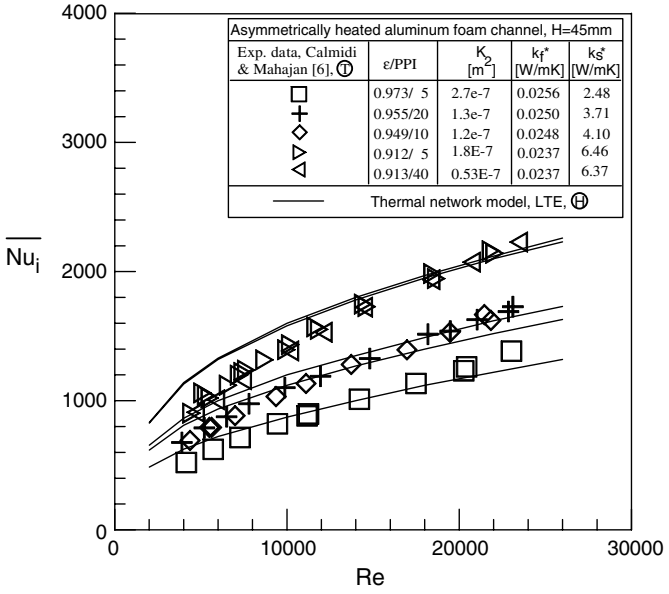

Fig. 5. Prediction of average Nusselt number in the Al-foam channel.

indicating that the presented numerical calculation is reasonable. Besides, Eq. (6), given in the section on the thermal network model can be determined from numerical solutions for slug flow. This data-fitting is accurate to within 1%. The correlation is applied to predict the heat transfer in porous channels.

4.2. Validity of thermal network model

This section addresses the validity of the thermal network model in porous channels by comparing its results with other experimental results. Fig. 4 plots the distribution of inlet Nusselt numbers in the streamwise direction for the sintered copper bead porous channel with uniform heat flux on the surface of the bottom wall of the channel. Calculations were made under the following conditions; channel height, $H = 10$ mm; medium porosity, $\varepsilon = 0.37$; permeability, $K = 2.9 \times 10^{-10}$ m^2; inertial coefficient, $C_F = 0.242$; Reynolds number, $Re = 889$–5556; effective fluid conductivity, $k_f^* = 0.01$ W/(m °C); effective solid matrix conductivity, $k_s^* = 10.57$ W/(m °C), and various interstitial heat transfer coefficients as presented in Table 1. The above values of the relevant parameters match those used in the experiments performed by Hwang et al. [4]. Fig. 4 reveals that the predictions obtained by applying the presented thermal network model are generally consistent with the experimental data of Hwang et al. [4]. The average deviation is 12.1%. The average inlet Nusselt number predicted using this thermal network model were also compared with the experimental data reported by Calmidi and Mahajan [6] for asymmetrically heated aluminum foam channels. Fig. 5 presents the comparison. The experimental data of Calmidi and Mahajan [6] for foam–air combinations indicate that the transport-enhancing effect of thermal dispersion is extremely weak, because the conductivity of the solid matrix is relatively high. It also shows that the interstitial heat transfer coefficient is sufficiently high to cause LTE. Therefore, the effect of pore density (PPI) on the Nusselt number is negligible. The predictions made using the thermal network model support this finding. The theoretical results appear to under-predict the experimental Nusselt number at high Reynolds number, and over-predict it at low Reynolds number. The former finding reveals that another transport-enhancing effect (such as turbulence) may occur, as reported by Calmidi and Mahajan [6]. The latter result follows from the differences between the thermal boundary conditions. The experiments of Calmidi and Mahajan [6] involved a quasi-uniform wall temperature boundary condition; whereas the thermal network model herein is based on a uniform wall heat flux boundary condition. The predictions made using the presented model are generally reasonable for asymmetrically heated aluminum foam channels. Hence, Figs. 4 and 5 demonstrate that the presented thermal network model can accurately predict the convection heat transfer in porous channels.

4.3. Identify inlet thermal boundary condition and LTE

Fig. 6 plots the distributions of bulk Nusselt numbers in the streamwise direction for $C_1 = 0$ or $C_1 =$ infinity at various h_v. The C_1 is a factor in the inlet thermal boundary condition that was described in the section on Boundary Conditions. When C_1 is zero, the gradient of the solid matrix temperature is also zero at the channel inlet. If C_1 approaches infinity, the LTE is between the solid matrix and the fluid at the channel inlet. These two values of C_1 are just the two limits in the boundary condition at the channel inlet. Calculations were made under the following

conditions; channel height, $H = 30$ mm; medium porosity, $\varepsilon = 0.875$; permeability, $K = 2.193 \times 10^{-8}$ m^2; inertial coefficient, $C_F = 0.162$; Reynolds number, $Re = 600$; effective fluid conductivity, $k_f^* = 0.0219$ W/(m °C); effective solid matrix conductivity, $k_s^* = 3.38$ W/(m °C), and various interstitial heat transfer coefficients, $h_v = 2.07 \times 10^2 - 2.07 \times 10^5$ W/(m^3 °C). Fig. 6 reveals that the prediction made using the thermal network model is between the numerical calculations obtained by applying the two limiting values of C_1. Moreover, the effect of C_1 on the numerical calculation becomes weaker as the interstitial heat transfer coefficient increases because the larger interstitial heat transfer coefficient corresponds to a shorter thermal entrance.

Fig. 6 also reveals that the predictions obtained using the presented thermal network model at local non-thermal equilibrium are reasonably between the numerical calculations made at $C_1 = 0$ and those made at $C_1 =$ infinity. These accurate predictions are successful until h_v rises to 2.07×10^5 W/(m^3 °C) because the porous channel with $h_v = 2.07 \times 10^5$ W/(m^3 °C) was in LTE. Therefore, the predicting model was changed from the one for local non-thermal equilibrium to that for LTE. How can the LTE be identified? The effective fin efficiency may be a useful index. When the effective fin efficiency is smaller, the thermal condition between the fluid stream and the solid matrix is nearer LTE. This work introduces a new parameter to specify the LTE. As stated in the section on the thermal network model and in Fig. 2, the overall heat transfer mechanism can be divided into two parallel heat transfer paths through which the channel wall transfers heat into the fluid stream. One is an indirect path through the solid matrix; the other is a direct path to the fluid stream. Theoretically, the heat transfer coefficient of the indirect heat transfer path is maximum when the thermal condition between the fluid stream and the solid matrix is in LTE. The relevant relationship is as follows:

$$\eta h_v H^* \leqslant h_b \frac{k_s^*}{k_f^* + k_d + k_s^*} \tag{31}$$

Substituting Eqs. (2)–(6) into Eq. (31) for thermal fully developed flow enables Eq. (31) to be reduced as follows:

$$\Omega = \left(\sqrt{\frac{h_v}{k_s^*}} H^*\right) \tanh\left(\sqrt{\frac{h_v}{k_s^*}} H^*\right) \leqslant 3 \tag{32}$$

Then, the value of Ω is used to specify LTE in porous channels. Under the LTE condition, Ω exceeds three; otherwise the thermal condition between the fluid stream and the solid matrix is at local non-thermal equilibrium. Fig. 7 presents the Ω as a function of Reynolds number for aluminum foam channels and sintered copper bead porous channels with different channel heights. The values of Ω were obtained by substituting h_v, k_s^* and H^* listed in Table 1 into Eq. (32). The experiments of Calmidi and Mahajan [6] on aluminum foam channels yielded a value of Ω that exceeds three. In other words, all they are LTE. This result is consistent with that of Calmidi and Mahajan [6], who found that the phases in their experiments were close to LTE. So the correlation for h_v, as posited by Calmidi and Mahajan [6], is unnecessary in their numerical simulations. A comparison with the results obtained by Hwang et al. [9] for an aluminum foam channel with $\varepsilon = 0.95$/10PPI and $H = 45$ mm reveals that the LTE conditions applied in the same Re region as identified by Calmidi and Mahajan [6]. However, Ω is much smaller than that of Calmidi and Mahajan [6]. The correlation for h_v presented by Hwang

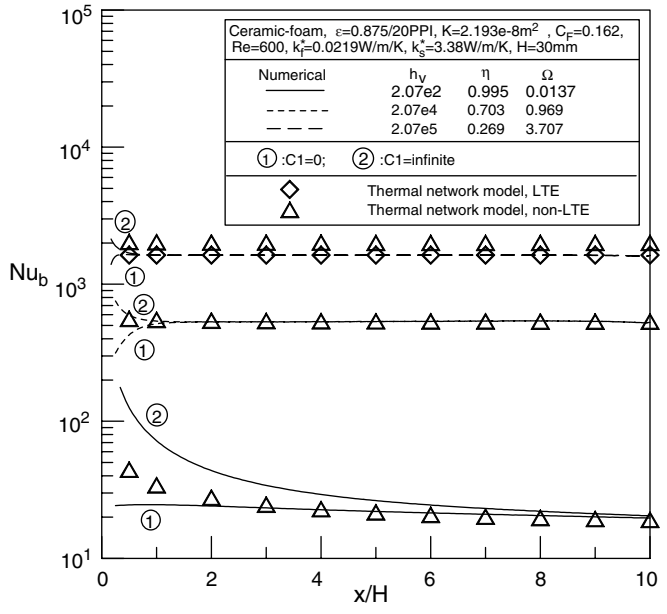

Fig. 6. Effect of C_1 on prediction of Nusselt number in the porous channel.

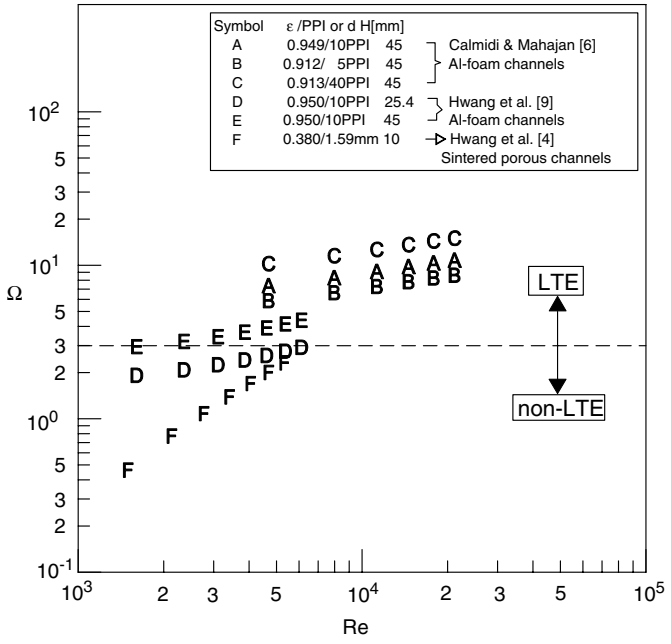

Fig. 7. Ω as a function of Reynolds number for various porous channels.

et al. [9] was determined by the single-blow method, which is the most popular experimental method for measuring h_v. The h_v correlation posited by Calmidi and Mahajan [6] may have been over-predicted. However, it does not influence the predicted thermal performance for aluminum foam channels with $\varepsilon \geqslant 0.91$, $H = 45$ mm and $Re \geqslant 4700$ because the phase is at LTE. Fig. 7 also reveals that Ω declines as the channel height (H) or Reynolds number falls, indicating that local non-thermal equilibrium may apply at small H and Re. For instance, the criterion for LTE in aluminum foam channels with $\varepsilon = 0.95$/10PPI and $H = 45$ mm is $Re \geqslant 1600$; but that with $\varepsilon = 0.95$/10PPI and $H = 25.4$ mm is $Re \geqslant 6600$. Fig. 7 plots the results obtained by Hwang et al. [4] for a sintered copper bead porous channel. The results in this work are consistent with those of Hwang et al. [4], who found that the LTE assumption was better justified at higher Reynolds numbers. This figure indicates that the criterion for LTE in sintered copper bead porous channels with $\varepsilon = 0.38/d = 1.59$ mm and $H = 10$ mm is around $Re \geqslant 6600$.

5. Conclusions

An algorithm model, which is simple and convenient for estimating the heat transfer of the porous heat sink in a channel, was successfully developed by applying the fin theory and thermal network concept. A comparison with numerical calculations and other experimental results validated that the presented algorithm model can accurately predict the convection heat transfer in various porous channels, such as metal foam channels and sintered porous channels.

The inlet thermal boundary condition was also investigated. Two limiting conditions applied at the channel inlet; (1) a zero gradient of the solid matrix temperature, and (2) LTE between the solid matrix and the fluid. The results show that the prediction made using the presented algorithm model is between the numerical calculations at the two limits. Additionally, the effect of the inlet thermal boundary condition on the numerical calculations becomes weaker as the interstitial heat transfer coefficient increases.

A parameter Ω in terms of h_v, k_s^* and H^* was postulated to specify the LTE in porous channels. When $\Omega > 3$, the phase is under the LTE condition, otherwise, it is under the local non-thermal equilibrium condition. Analytical results reveal some criteria for LTE in various porous channels. For instance, the criterion for LTE in aluminum foam channels is: if $\varepsilon = 0.91$ and $H = 45$ mm, $Re \geqslant 4700$; if $\varepsilon = 0.95$/10PPI and $H = 45$ mm, $Re \geqslant 1600$; if $\varepsilon = 0.95$/10PPI and $H = 25.4$ mm, then $Re \geqslant 6600$. Besides, the scope of LTE in sintered copper bead porous channels with $\varepsilon = 0.38/d = 1.59$ mm and $H = 10$ mm is about $Re \geqslant 6600$. Our results further demonstrate that Ω decreases as the channel height (H) or Reynolds number declines. Therefore, the phase in local non-thermal equilibrium could occur at a small H and Re.

Acknowledgements

The authors would like to thank the National Science Council of the Republic of China for financially supporting this research under Contract No. NSC 92-2212-E-344-005.

References

[1] M.L. Hunt, C.L. Tien, Effects of thermal dispersion on forced convection in fibrous media, Int. J. Heat Mass Transfer 31 (1988) 301–309.
[2] F.C. Chou, W.Y. Lien, S.H. Lin, Analysis and experiment of non-Darcian convection in horizontal square packed-sphere channels—1. Forced convection, Int. J. Heat Mass Transfer 35 (1992) 195–205.
[3] G.J. Hwang, C.H. Chao, Heat transfer measurement and analysis for sintered porous channels, ASME J. Heat Transfer 116 (1994) 456–464.
[4] G.J. Hwang, C.C. Wu, C.H. Chao, Investigation of non-Darcian forced convection in an asymmetrically heated sintered porous channel, ASME J. Heat Transfer 117 (1995) 725–732.
[5] K. Ichimiya, A new method for evaluation of heat transfer between solid material and fluid in a porous medium, ASME J. Heat Transfer 121 (1999) 978–983.
[6] V.V. Calmidi, R.L. Mahajan, Forced convection in high porosity metal foams, ASME J. Heat Transfer 122 (2000) 557–565.
[7] J.P. Holman, Heat Transfer, eighth ed., The McGraw-Hill Companies, Inc., New York, 1997, pp. 53–60.
[8] P.J. Roache, Computational Fluid Dynamics, Hermosa, Albuquerque, New Mexico, 1972, pp. 139–173.
[9] J.J. Hwang, G.J. Hwang, R.H. Yeh, C.H. Chao, Measurement of interstitial convection heat transfer and frictional drag for flow across metal foams, ASME J. Heat Transfer 124 (2002) 120–129.
[10] L.B. Younis, R. Viskanta, Experimental determination of the volumetric heat transfer coefficient between stream of air and ceramic foam, Int. J. Heat Mass Transfer 36 (1993) 1425–1434.
[11] V.V. Calmidi, R.L. Mahajan, The effective thermal conductivity of high porosity fibrous metal foams, ASME J. Heat Transfer 121 (1999) 466–471.
[12] S.L. Lee, A strong implicit solver for two-dimensional elliptic differential equations, Numer. Heat Transfer Part B 16 (1989) 161–178.
[13] R.K. Shah, A.L. London, Laminar Flow Forced Convection in Ducts, Supplement 1 to Advances in Heat Transfer, Academic Press, New York, 1978, p. 182.